UC Berkeley

UC Berkeley Previously Published Works

Title

Dynamic tunability of phase-change material transition temperatures using ions for thermal energy storage

Permalink

https://escholarship.org/uc/item/47m2418k

Journal

Cell Reports Physical Science, 2(10)

ISSN

2666-3864

Authors

Lau, Jonathan
Papp, Joseph K
Lilley, Drew
et al.

Publication Date

2021-10-01

DOI

10.1016/j.xcrp.2021.100613

Peer reviewed

eScholarship.org Powered by the California Digital Library
University of California

Cell Reports
Physical Science

CellPress
OPEN ACCESS

Article

Dynamic tunability of phase-change material transition temperatures using ions for thermal energy storage

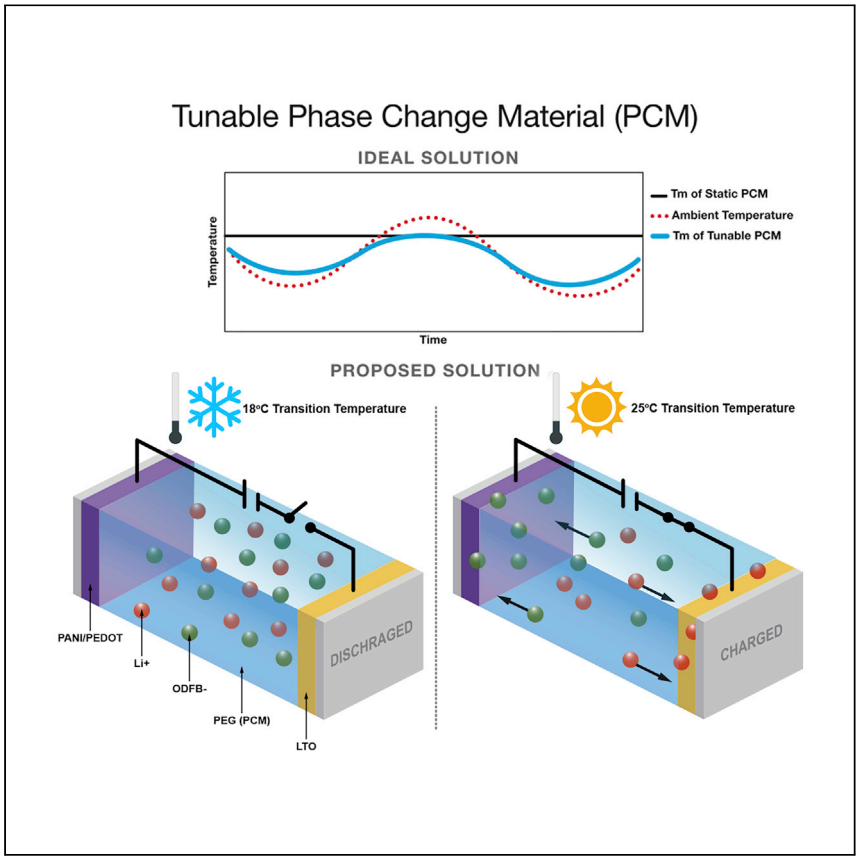

Lau et al. develop a dynamic tunable phase-change material (PCM) that uses ions to tune the T_m, based on the dual-ion battery concept. With static T_m PCM, utilization at ambient temperature is limited, whereas for tunable PCM, where T_m closely aligns with ambient temperature, higher energy storage is possible.

Jonathan Lau, Joseph K. Papp, Drew Lilley, ..., Christopher Dames, Gao Liu, Ravi Prasher

gliu@lbl.gov (G.L.)
rsprasher@lbl.gov (R.P.)

Highlights

Dynamically tunable T_m (15°C–21°C) of phase change materials with 2.5 V perturbation

A dual-ion battery approach using ions to modulate T_m of the phase-change materials

Combination of thermal energy storage with electrical energy storage in one device

Demonstration of higher thermal utilization of the dynamically tunable PCM

Lau et al., Cell Reports Physical Science 2, 100613
October 20, 2021 © 2021 The Authors.
https://doi.org/10.1016/j.xcrp.2021.100613

Cell Reports
Physical Science

CellPress
OPEN ACCESS

Article

Dynamic tunability of phase-change material transition temperatures using ions for thermal energy storage

Jonathan Lau,[1,3] Joseph K. Papp,[1,3] Drew Lilley,[1,2] Piyachai Khomein,[1] Sumanjeet Kaur,[1] Christopher Dames,[1,2] Gao Liu,[1,*] and Ravi Prasher[1,2,4,*]

SUMMARY

Thermal energy storage (TES) based on phase-change materials (PCMs) has many current and potential applications, such as climate control in buildings, thermal management for batteries and electronics, thermal textiles, and transportation of pharmaceuticals. Despite its promise, the adoption of TES has been limited, in part due to limited tunability of the transition temperature, which hinders TES performance for varying use temperatures. Transition temperature tuning of a material using an external stimulus, such as pressure or an electric field, typically requires very large stimuli. To circumvent this problem, here, we report on the dynamic transition temperature tunability of a PCM using ions. We achieve a transition temperature tunability up to 6°C in polyethylene glycol (PEG) by using the salt lithium oxalatodifluoroborate at a low voltage of 2.5 V, which may enable simpler and safer devices/system designs. We also explain the thermal properties of the salt/PCM solution using the Flory-Huggins theory.

INTRODUCTION

It is abundantly clear that deeper penetration of renewable electricity is only possible by further developing scalable, affordable, and sustainable energy storage.[1] Since no single solution can satisfy all of the diverse application needs to decarbonize the world, various types of energy storage technologies,[2] such as electrochemical, thermal, and mechanical, are under investigation. Phase-change material (PCM)-based thermal energy storage (TES) is of particular interest in many applications, such as buildings[3] and thermal textiles,[4] to provide localized and personalized cooling/heating, dry cooling of power plants[5] to conserve water by using the diurnal swing of ambient temperature; thermal management of batteries and microelectronics,[6] and transportation of foods, pharmaceuticals and medical supplies.[7–9] In all of these applications, the PCM works near the ambient temperature and is typically designed to operate at a fixed temperature.

One fundamental challenge in the adoption of PCM-based TES is that there is limited tunability in the usage temperature. Unlike an electrochemical energy storage device where the voltage is fixed, as with a Li-ion battery, the variation in ambient temperature means that the thermal voltage (i.e., the temperature) is not fixed for the near-ambient applications mentioned above. For example, the use temperature during summer and winter months (Figure 1A) can vary significantly (there can be also significant diurnal variations). In reality, that translates into reduced use of the PCM, because either the PCM melts partially or does not melt at all.[10] To solve

[1]Energy Storage & Distributed Resources, Lawrence Berkeley National Laboratory, Berkeley, CA 94720, USA

[2]Department of Mechanical Engineering, University of California, Berkeley, Berkeley, CA 94720, USA

[3]These authors contributed equally

[4]Lead contact

*Correspondence: gliu@lbl.gov (G.L.), rsprasher@lbl.gov (R.P.)

https://doi.org/10.1016/j.xcrp.2021.100613

This is an open access article under the CC BY license (http://creativecommons.org/licenses/by/4.0/).

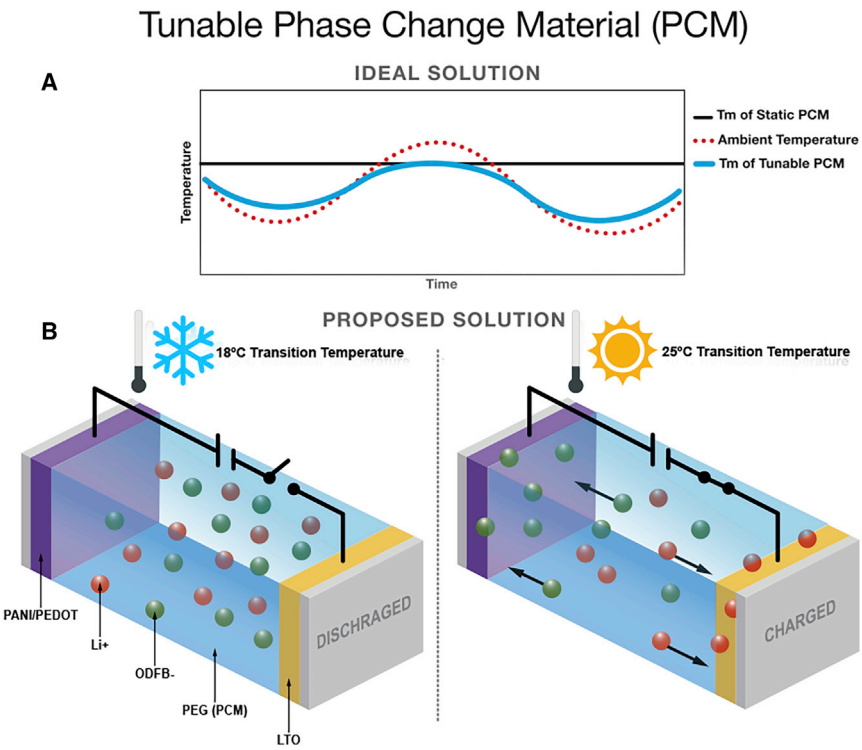

Figure 1. Dynamically tunable PCM-based TES device enhances the thermal storage efficiency

(A) A schematic depicting impact of changing ambient temperature (either diurnally or seasonally) on utilization of static and tunable TES exposed to ambient temperatures. If the ambient temperature is too cold as compared to the transition temperature of the static PCM, then no phase change will take place. If the ambient temperature is too hot as compared to the transition temperature, then the PCM will very quickly change phase, melt, and remain in the molten state without providing much benefit. Therefore, ideally the transition temperature of PCM should be closely matched with the ambient temperature.

(B) Schematic of the dual-ion battery for dynamic tunability of the PEG PCM TES developed in this study.

this problem, use of multiple combined PCMs with different melting temperatures has been proposed, which increases the cost.[11]

There has been significant interest in recent years in making thermal materials and devices tunable, such that their properties and performance can be dynamically changed.[12,13] However, most of the focus has been on changing thermal transport properties, such as thermal conductivity,[12,13] rather than thermodynamic properties, such as the melting/transition temperature (T_m) of a material. Changing the T_m of a material dynamically using an external stimulus such as pressure,[14] an electric field,[15] or a magnetic field,[16] is a non-trivial task, as the required magnitude of the stimulus to achieve a sizable change in T_m is typically large, and the enthalpy change at T_m is only moderate for thermal storage applications. One recent example of transition temperature tuning involved the use of an optically controlled mechanism.[17,18] In that work, tuning was to achieve different transition temperatures for charging the PCM with thermal energy and discharging the transition temperature; this enables a reduction of heat loss from the PCM and can eliminate the need for thermal insulation. However, to dynamically tune the transition temperature, in which both charging and discharging of thermal energy happens at the same temperature using nominal stimulus continuously, depending on the conditions, is still elusive. A recent

CellPress
OPEN ACCESS

commentary[19] on five thermal energy grand challenges for decarbonization highlighted the development of tunable T_m as one of its challenges.

In this article, we report on the dynamic tunability of T_m of a PCM using ions with very modest voltage requirements. While it is well known that the addition/removal of salt changes the melting temperature of a solution,[20,21] dynamic modification of the salt concentration is nontrivial, and the requirement for reversibility and long-term cyclability precludes the use of physical or chemical separation techniques in modular applications. To overcome these challenges, we have used a dual-ion battery (DIB)[22,23] as shown in Figure 1B to electrochemically modify the concentration of salt in a PCM and its T_m in a reversible and dynamic manner. In a DIB, a PCM with a high initial salt concentration and low T_m serves as the electrolyte for the device. Electrochemical charging stores the cations and anions in the negative and positive electrodes, respectively. This decreases the nominal salt concentration in the PCM/electrolyte itself, raising its T_m. The device can then be electrochemically discharged to reverse the process and lower the T_m to its original value.

The state of charge (SOC) controls the magnitude of T_m. DIBs store cations and anions from the bulk electrolyte via redox reactions.[22] This enables much higher charge storage capacities and greater changes to the salt concentration (i.e., T_m) of the bulk electrolyte in DIBs. The storage of ions via faradic reactions also reduces the self-discharge of the device and may obviate the need for a constant applied voltage to maintain a chosen T_m.[24,25] It should be noted that DIBs are fundamentally different compared to rocking-chair devices (e.g., Li-ion batteries) in which cations (e.g., Li^+) are typically passed from one electrode to the other through the electrolyte upon charge or discharge.[26] In such devices, electrochemical cycling does not change the bulk electrolyte concentration.

For a DIB to work as a dynamically tunable TES device, there are three components—PCM, salt, and electrodes—that need to be selected and manipulated for optimized performance. Here, we detail our selection criteria and design rules for salt selection.

RESULTS AND DISCUSSION

PCM selection

Several requirements guide the selection of the PCM for dynamic tunability of the T_m: (1) moderate to large enthalpy change at T_m; (2) the ability to solvate salts and provide sufficient ionic conductivity for electrochemical device operation[27]; (3) sufficiently low electronic conductivity so that self-discharge through the material is minimized[27]; and (4) the T_m of the PCM should be close to room temperature so that the tunable range of T_m is relevant for near-ambient applications. Polyethylene glycol (PEG) has an enthalpy change of ~100–150 kJ/kg,[28] satisfies the electrical considerations, and has been explored as polymer electrolytes for batteries.[27] While less commonly used for electrochemical applications, molecular weight (M_n) varieties of the polymer near 1,000 g mol^{-1} possess T_m near room temperature.[29] PEG with M_n ~1,000 g mol^{-1} is thus uniquely suited as an electrochemically compatible PCM for the dynamic tunability of the T_m, and is used exclusively in this study.

Salt selection using static experiments

To develop design rules for optimal salt-PEG systems that maximize T_m tunability and lead to stable solutions, we conducted experiments with five salts: Li oxalatodifluoroborate (LiODFB), LiI, Li bis(trifluoromethanesulfonyl)imide (LiTFSI), CsTFSI, and 1-butyl-1-methylpyrrolidinium bis(trifluoromethylsulfonyl)imide-PEG (Pyr_{14}TFSI-PEG)

(see Method details). Static experiments in which the thermodynamic properties (enthalpy change and T_m) were measured for different concentrations of these various salts-PEG systems were performed to help design the dynamic experiments using DIB.

Differential scanning calorimetry (DSC) thermograms of the LiODFB-PEG samples are shown in Figure 2A. Increasing salt concentrations shifts the peak T_m to lower temperatures. However, the broad transition peaks make the typical determination of the onset temperature via extrapolation of the peak tangent inappropriate, as it neglects partial melting of the material at lower temperatures. Instead, the temperature corresponding to a prescribed fraction of the total enthalpy of phase transition better characterizes the system. For salt selection, the temperature corresponding to 50% of the total enthalpy change (referred to as T_{50}) was used (Figure 2B). Similarly, T_{10} denotes the temperature corresponding to 10% of the total enthalpy change. The T_{50} transition temperatures were used to better understand the changes in the bulk melting rather than the onset temperatures. The broad transition peaks observed via DSC (e.g., T_{10}–T_{90} ranging from ~10°C –17°C for LiODFB-PEG in Figure 2A), indicate a distribution of melting temperatures and/or slow kinetics of phase transition. Step scans were carried out to elucidate the nature of these broad transition peaks as seen in Figure S1. The measurements confirm that the breadth of the peak is not due to kinetic limitations, because the transformations remain incomplete even when the temperature is held above the T_m. Reconstructed thermograms from the step scans are also shown to closely follow the DSC thermograms measured at 10°C min^{-1} (Figure S2), which indicates that the melting behavior of the samples is largely independent of the ramp rate. This suggests that the broad peaks are due to a distribution of melting temperatures, which is commonly encountered in polymers.[30–32] While this can lead to inefficiencies in thermal energy storage applications, the transition peak breadth may be narrowed with the use of monodisperse PEG.

Figure 2C shows an obvious decrease in T_{50} with increasing anion size (where the size of I^- << $ODFB^-$ < $TFSI^-$), whereas there is no clear trend (Figure 2D) for cation size (where the size of Li^+ < Cs^+ << Pyr_{14}^+). The largest cation and anion pair in Pyr_{14}TFSI shows only a minor change in the transition temperature; similarly, the smallest pair (LiI) also shows only a very modest change in T_{50}.

Flory-Huggins theory (FHT), which is used to understand the thermal properties of salt/polymer solutions,[33] is applied here to provide additional context to the T_{50} data (see Method details). A large negative value of χ (the interaction parameter) in FHT means a higher solubility of the salt in the polymer, which is expected to lead to greater degrees of T_m depression. Figure 2E shows the fitted χ (see Method details) as a function of ratio ($R = r_{cation}/r_{anion}$) of cation to anion radii. The large $\chi \sim -8$ for alkali salts, $LiODFB^-$, $LiTFSI^-$, and $CsTFSI^-$ is supported by the formation of polyethylene oxide (PEO):X complexes observed in these systems.[28] This indicates that smaller R may be better for T_m control as it leads to larger χ. Conversely, if R increases due to a relative increase in the cation size, χ becomes less negative (sometimes positive), leading to a decreased salt solubility and less sensitive T_m depression. Both Pyr_{14}TFSI and LiI have larger values of R (Table S1), resulting in less sensitivity of T_m (Figures 2C and 2D; Note S1). These results are discussed further in Figure S3, which shows the interaction parameter fits of the LiODFB-, LiTFSI-, CsTFSI-, and Pyr_{14}TFSI-PEG systems using the T_{50} temperatures of different static compositions.

As just discussed, small R resulting in high solubilities of some alkali salts is ideal for maximizing the T_m tunability of the PEG PCM. For the purposes of electrochemical

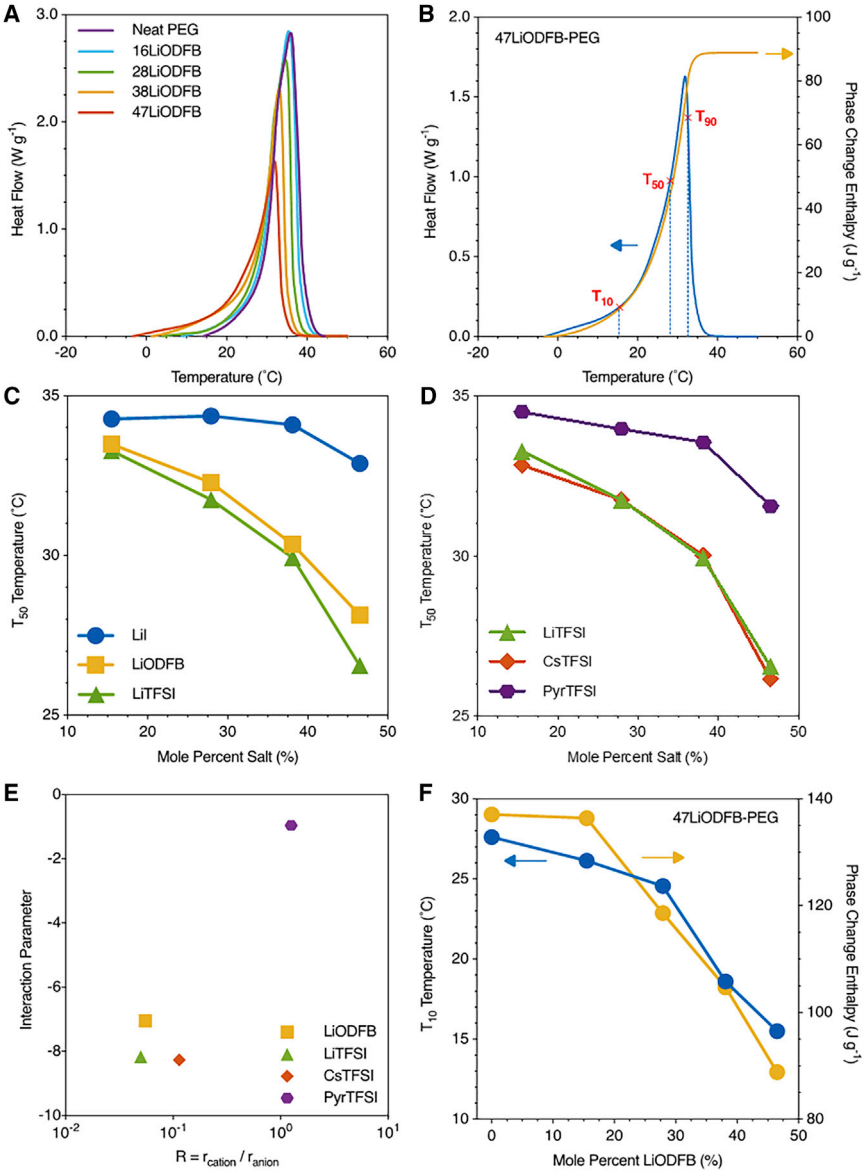

Figure 2. Thermal measurements results of the impact of ions on the thermal physics properties of the PEG-based PCM

(A) DSC thermograms of LiODFB-PEG samples with concentrations ranging from 0 to 47 mol% measured at a ramp rate of 10°C min^{-1}, as encoded in the caption by the 2-digit number before LiODFB.

(B) DSC thermogram and running enthalpy for 47LiODFB-PEG. The red crosses on the blue thermogram that curve from left to right represent T_{10}, T_{50}, and T_{90}, respectively.

(C and D) T_{50} of salt-PEG system with identical cation and different anion sizes (C) and (D) T_{50} of salt-PEG system with different cation sizes and identical anion.

(E) Interaction parameter of the different salt-PEG systems as a function of r_{cation}/r_{anion}.

(F) Comparison of the T_{10} (signifying onset of melting) and phase-change enthalpies of the LiODFB-PEG samples. The addition of LiODFB depresses both T_m and phase-change enthalpy of PEG with increasing salt concentrations; from 27.6°C to 15.5°C and 137.1 to 88.8 J g^{-1} in neat PEG and 47LiODFB-PEG, respectively.

modulation of the salt concentration in the PCM, the salt must also be compatible with the electrode chemistries and other system requirements. Of the Li salts investigated, LiODFB was chosen as the salt for a DIB device due to its high solubility, high thermal stability, and ability to passivate Al current collectors.[34] Various LiODFB-PEG samples ranging from 0 to 47 mol% LiODFB were synthesized and characterized (see Method details). Higher concentrations of LiODFB-PEG are liquid at room temperature and were omitted from further study.

T_{10} (signifying the onset of melting) results are reported in the rest of the article. T_{10} and enthalpies of transformation of the LiODFB-PEG samples are shown in Figure 2F, and the precise numerical values are tabulated in Table S2, along with T_{50} and T_{90}. The addition of LiODFB is shown to depress both the T_m and phase-change enthalpy of PEG with increasing salt concentrations. A similar trend in the phase-change enthalpy with increasing salt concentration was previously observed in the LiTFSI-PEO system.[33] The loss in phase-change enthalpy with the incorporation of salt is due to a decreasing weight fraction of PEG in the salt-PEG system (the LiODFB salt itself does not contribute to the enthalpy of transition at the temperatures of interest). Nonetheless, over the composition range studied, the LiODFB-PEG system demonstrates a potential tunable T_m window of $\Delta T_{10} = 12.1°C$ and highlights the validity of using salt to modulate the thermal properties of a PCM.

Electrode selection and electrochemical system engineering

Over the past 40 years, the PEO electrolyte-based solid-state battery (SSB) has advanced to the point that it may power electric vehicles for hundreds of miles per charge, and can withstand thousands of charge/discharge cycles over a lifetime of nearly 10 years. (Note that high-molecular-weight PEG is commonly referred to as PEO; this study uses low to medium molecular weight, referred to as PEG.[35–37]) Our tunable TES device shares the basic PEG materials and similar Li salts with the PEG-based SSB. Moreover, the tunable TES device shares the same structure as the PEG-based SSB (Figure S4), but has drastically different challenges for this unique electrochemical system. Two distinctive challenges differing from SSB are highlighted here, leading to our unique material choices and device architectures. For tunable PCM, enthalpy change during thermal transition is more critical, as it is enthalpy change that decides the thermal energy density, whereas for batteries, higher voltage is more important, as it is voltage that determines the electrical energy density. In tunable TES, the voltage is used as a stimulus to insert ions to change T_m. Therefore, low voltage is preferred for the tunable TES device.

The low voltage of $\leq$2.5 V is preferred for the PEG-based PCM, as PEG will chemically disintegrate above 3.8 V versus Li/Li^+, making PEG a disadvantaged property for battery applications but ideal for tunable TES applications.[27,38] The electrode materials selection choices would be a lower potential cathode material, and a higher potential anode material, to yield a low-voltage tunable TES device that has thermodynamically stable interfaces to ensure operational longevity. In this case, Li titanium oxide $Li_4Ti_5O_{12}$ (LTO) is selected as an anode active component to store and release Li ions. LTO is a perfect choice as an anode material, as its operational potential is flat ~1.55 V versus Li/Li^+ (Figure S5). The PEG-based PCM electrolyte is both electrochemically and chemically stable toward LTO at this potential to ensure a thermal dynamically stable interface—therefore, no interfacial decay over the long period of operation.[35,39] The conventional Li-ion or Li-PEG polymer battery is operated well below the stability limit (0.8 V versus Li/Li^+) of the PEG electrolyte. As reported, most of the Li-ion battery decay comes from the low potential anode and electrolyte interface failures, due to the solid electrolyte interphase (SEI)

formation and breakdown over the lifetime of the battery. Rechargeable batteries based on LTO anodes have demonstrated millions of cycles with very little interface and materials decay. The unique low voltage requirements of the tunable TES device make the LTO an ideal anode choice. Since electrical energy storage is not a paramount requirement for the tunable TES device, the overall cell voltage is preferably low for simple operation. Low-potential cathodes, which are out of favor for battery applications, are preferred here to achieve the low-voltage tunable TES device; lower potential cathodes (below 3.8 V operational potential) stay within the electrochemical and chemical stability window of the PEG electrolyte to significantly improve the long-term stability of the TES device. In addition, the PCM PEG electrolyte may have much higher oxidation stability—up to 4.5 V Li/Li^+ at a higher salt concentration of 47% LiDOBF.[40] This higher voltage stability opens up new possibilities for other high-capacity cathode materials for the tunable PCM device, and may provide better electrical energy storage capability. Although the tunable TES device is an electrochemical cell, unlike the Li-ion battery operated beyond the thermal dynamic stability window of its electrolyte, the tunable TES device can use materials within their thermal dynamic stability window during device operation, so it can have a much longer life and perform more cycles compared to that of the best Li-ion battery (Figure S6).

The second major difference is that the cathode needs not to intercalate and deintercalate Li cations, compared to the Li rechargeable battery, but to absorb and release anions of the corresponding salt in the PCM electrolyte (Figure 1B). In most of the Li-ion batteries, a transition metal oxide cathode is used to house Li cations; among the transition metals, Ni and Co are the primary choices. In the DIB design for the tunable TES device, the Li salt needs to be removed from or released to the PCM electrolyte during cycling.[22,23,41,42] Since the LTO anode is housing Li cations, the cathode is used to host anions such as $ODFB^-$. The function of the cathode can be achieved by a redox active polymer[43,44] instead of transition metal oxide-based ceramic materials. The advantages of using redox polymers are many, including lower potentials of redox activities to achieve a lower device voltage and better PCM stability, no use of constrained resource materials, and a large variety of choices of redox materials based on the diverse carbon chemistries, as well as easy processing into film laminate and device integration. However, redox polymers are not without challenges; as compared to ceramic materials, organic redox materials are prone to isomerize and transform during repeat oxidation and reduction. In line with this, two types of redox organics are used and reported here. One is the classic polyaniline (PANI) conductive polymer material.[43,44] The PANI is low cost, is made in commercial scale, has lower oxidation potential, and is stable toward oxidation (Figure S7). The PANI-carbon black-based anode electrode demonstrates excellent capacity stability toward oxidation and reduction during the >70 cycles tested (Figure 3B). The initial capacity improvement is due to the continuous wetting of the PANI cathode materials by PEG electrolyte to improve the anion accessibility to the oxidation sites of the PANI. The PANI electrode potential also stabilizes after the initial cycling; extended cycling is being tested to further gauge its performance. Another popular redox material, poly(3,4-ethylenedioxythiophene) (PEDOT), is also tested for the cathode application (Figures S8–S12; Note S2). The PEDOT-carbon nanotube electrode functions similarly to the PANI-CB electrode to reversibly oxidize and host $ODFB^-$. However, compared to the PANI, the PEDOT is less stable with the PCM electrolyte. The performance differences between the two organic redox cathodes demonstrate not only the universal feasibility of the DIB approach for tunable PCM applications but also that there is more materials engineering to be done to achieve superb PCM device stabilities.

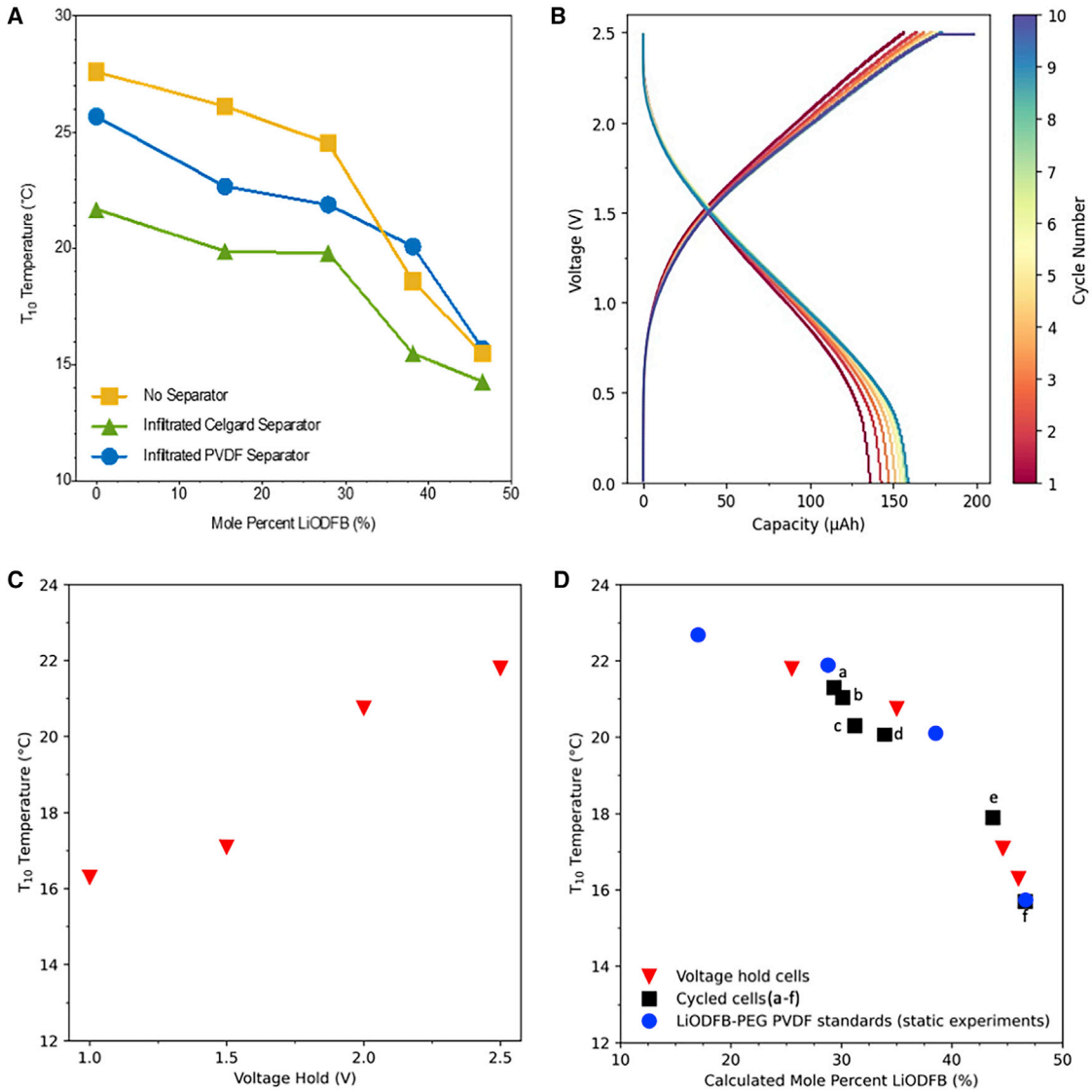

Figure 3. Use voltage or capacity dial to tune the T_m of the PCM based on dynamically tunable TES device via a dual-ion battery chemistry

(A) T_{10} as a function of LiODFB-PEG composition (obtained using static experiments) with and without polymer separators. Samples with polymer separators were prepared by infiltrating melted LiODFB-PEG into either polypropylene Celgard or PVDF separators. Comparing these curves shows a decrease of 1.9°C in the T_{10} of neat PEG (zero salt concentration) upon infiltration into PVDF, compared to a decrease of 5.9°C upon infiltration into Celgard. PVDF separators are used in the prototype devices (called PVDF standards hereafter) due to the larger T_{10} swing as a function of LiODFB concentration, by 10°C. This tunability range for PVDF standards also is centered more usefully around ambient temperatures compared to the T_{10} range of Celgard separators.

(B) Galvanostatic profile for a cell cycled 10 times. The figure shows measured galvanostatic profile of the full cell cycled at a rate of C/4 with respect to the PANI electrode. Note that charge means that salts are being removed from the PEG and stored in the electrodes, and discharge means the opposite. Therefore, a charge capacity of zero means the highest salt concentration in the PEG.

(C) T_{10} of LiODFB-PEG-infiltrated PVDF separators in pre-conditioned (cycled 5 times) cells followed by a set voltage hold for 10 h, as determined by *ex situ* DSC on the harvested separators.

(D) T_{10} of LiODFB-PEG-infiltrated PVDF separators in voltage hold and cycled full cells as a function of estimated mole percent LiODFB, compared to the LiODFB-PEG PVDF standards. This series of cycled cells are labeled as follows: (a) cycled 19 times, charged to 2.49 V; (b) cycled 12 times, charged to 2.49 V; (c) cycled 11 times, charged to 2.35; (d) cycled 9 times, charged to 1.9 V; (e) cycled 9 times, charged to 1.1 V; (f) cycled 0 times, not charged. Charge capacity is converted to mole percent LiODFB in the PEG using the formula given in Method details. T_{10} from dynamic experiments match very well with the LiODFB-PEG PVDF standard results obtained using static experiments from (A). The lowest mole percent achieved in dynamic experiments was ~25%, as compared to 0% in static experiments.

Demonstration of dynamic tunability using DIB

With the salt selection decided from the static experiments and electrode couple selection from electrochemical evaluation, here, we discuss our experiments that show the dynamic tunability of T_m using ions in a DIB. The DIB (Figure 1) consists of an LTO^- electrode, PANI-CB^+ electrode, and 47LiODFB-PEG infiltrated into a polymer separator (not shown in Figure 1B) for mechanical support (see Method details). While graphite-graphite symmetric cells are archetypal of DIBs, the potentials required for Li^+ and anion intercalation into graphite (0.01 and ~5 V versus Li/Li^+, respectively) induce significant electrochemical degradation of the polymer electrolyte.[23,42] Initial investigations of potential electrodes also showed the undesirable co-intercalation of the PEG with Li^+ into graphite. LTO was chosen as the negative electrode due to its higher redox potential for Li^+ intercalation (1.55 V versus Li/Li^+, which is within the electrochemical stability window of PEG as shown in Figures S4 andS5), and the inability of PEG to co-intercalate into its crystal structure. PANI was similarly chosen as the positive electrode due to the lower redox potential for anion doping (<3.8 V versus Li/Li^+),[45] and carbon black was used to increase electronic conductivity. PANI is a conjugated polymer that is able to accommodate cations or anions through an electrochemical doping/de-doping process via redox of the aniline moieties along the polymer backbone at low and high potentials, respectively. The galvanostatic profile of the synthesized PANI-CB composite is shown in Figure S7. An upper voltage limit of 3.4 V versus Li/Li^+ was implemented for the PANI-CB electrode to reduce the electrochemical oxidation of PEG in the device (~3.8 V versus Li/Li^+).[46] To compensate for the low specific capacity of 40–60 mAh g^{-1} for the PANI, high mass loading electrodes were fabricated using stainless-steel mesh current collectors. Cells were also constructed using alternative electrode materials, including PEDOT and carbon nanotubes (CNTs) to demonstrate customizability of the system to optimize the DIB (Figures S8–S12).[47] The PEDOT-CNT demonstrated significant tunability (Figures S10–S12), but lacked high efficiencies (Figure S9) and economic feasibility. Therefore, only the PANI-CB results are shown in the main text. The schematic of electrode and cell fabrication is shown in Figure S4.

A polymer separator is used to provide mechanical support and prevent short-circuiting of the electrodes, but it can also significantly affect the thermal properties of the device, and therefore needs to be carefully selected. T_{10} of the different LiODFB-PEG compositions (obtained using static experiments) with and without polymer separators are shown in Figure 3A. A polypropylene Celgard separator (40 μm thick, 20 nm pore diameter) lowers the transition temperature of LiODFB-PEG across the entire composition range studied. A polyvinylidene fluoride (PVDF) separator (125 μm thick, 220 nm pore diameter) also contributes to a lowering of the $T_{10,}$ but to a lesser extent. It is hypothesized that the pores of the polymer separators restrict the size of the crystalline domains of PEG, and the smaller resultant domains possess lower melting points.[30–32,48] The 220-nm pores of the PVDF separator thus influence the transition temperature to a lesser extent than the 20-nm pores of the Celgard separator. PVDF separators are used in the prototype DIB devices due to the larger range of T_{10} as a function of salt concentration seen in these static tests. The LiODFB-PEG infiltrated PVDF separator samples are used to compare the thermal properties of the dynamically tuned PCM, and are hereafter referred to as PVDF standards.

The maximum operating voltage of the full cells was determined from the half-cell (Figures S5 and S7) characterization of the LTO and PANI electrodes. The capacity of the PANI electrode is limiting and allows for the use of the lithiation plateau of

LTO to pin the full-cell upper voltage limit to 2.5 V. A representative galvanostatic profile of a full cell cycled at a rate of C/4 with respect to the PANI electrode is shown in Figure 3B. The Coulombic efficiency in the full cells increases steadily with cycling but plateaus to ~90% after 5 cycles. Low efficiencies are also observed in LTO-based Li-ion batteries, and are attributed to side reactions of carbonate-based electrolytes catalyzed by TiO_2 impurities and/or the LTO surface.[49] However, the nature and extent of these reactions with PEG polymer electrolytes is not well understood.

Ex situ thermal characterization was performed on the LiODFB-PEG-infiltrated PVDF separators harvested from full cells charged to different capacities (or SOCs). T_{10} as a function of voltage holds (and associated charged capacity) of the cells is shown in Figure 3C for the LTO/PANI-CB device, whereas T_{50} and T_{90} information is reported in Figures S13 and S14, respectively. For comparison, T_{10} as a function of voltage holds an associated charged capacity for the LTO/PEDOT-CNT device, and analogous results for T_{50} and T_{90} are given in Figures S10, S11, and S12, respectively. Very modest applied voltages (<2.5 V) performed after conditioning the system for 5 cycles resulted in a T_{10} swing of nearly 6°C. Figure 3D shows the same data as in Figure 3C, but as a function of LiODFB-PEG composition in the separator (see Method details) and with additional data points (static experiment standards and more cycled cells) for reference. Cells cycled 15–25 times between 0 and 2.5 V at C/4 were harvested at various points to determine the impact of multiple cycling on T_m. The T_{10} from the dynamic experiments, both voltage holds and cycling, match closely with T_{10} from static experiments. Fully discharged cells after conducting the cycling experiments show an average T_{10} of 16.3°C that closely match the average T_{10} of 15.7°C for the 47LiODFB-PEG PVDF standards from static experiments (Figures 3A and 3D at 47 mol%). This value is close to that which is expected, given the net zero change in the PCM salt concentration assumed in these devices. This indicates that the process of electrochemical cycling does not significantly alter the thermal properties of LiODFB-PEG, even considering the coulombic efficiency of cycling. Cycled cells with <30 mol% LiODFB do display a slightly smaller T_{10} than the corresponding standards, indicating that the salt extraction estimation for many cycled cells may have increased error. However, the characterization of cycled cells shows the expected general trend of T_{10} dependence on SOC. Cycled cells were harvested with charged capacities between 0 and 202 μAh and demonstrated a total T_{10} swing of >5°C; these results are remarkable in that only quite modest voltages (~2 V) were used to achieve this tunability of phase transition temperature, which has significant technological implications as it will allow for simpler and safe system design. In practice, depending on the required T_m (which, in turn, will depend on the changing ambient conditions and frequency with which T_m change is required, e.g., diurnal versus seasonal), one can use the appropriate voltage based on data shown in Figure 3C. The tunable PCM device is working at an ambient condition, in which the temperature of the electrodes fluctuates. Due to the thermogalvanic effect,[50,51] the overall cell voltage can drift by a few hundred millivolts, depending on the ambient temperature at a given salt concentration in the PCM. To achieve precise control of the ion concentration, cell voltage needs to be calibrated and adjusted with ambient temperature.

Energy efficiency of the device

The thermal and electrochemical energy of the prototype devices can be estimated from the cell build and electrochemical cycling. Considering cell a in Figure 3D as a representative device, the electrically discharged cell (47 mol% LiODFB) has 16 mg LiODFB-PEG loaded in the PVDF separator and can store 1.4 J thermal energy via its phase transformation (Figures 2F and S15) with a T_{10} of 15.5°C (Figures 3C and 3D).

CellPress
OPEN ACCESS

The salt concentration is reduced in the PEG in the electrically charged state (~47 mol% LiODFB), and the cell has ~1.7 J (Figures 2F and S15; Note S3) thermal energy storage with a T_{10} of 22.0°C (Figures 3C and 3D, cell a). The cell requires 1.4 J electrical energy to charge the device, and ~0.7 J electrical energy can be recovered upon discharge with a round-trip energy electrical efficiency of ~50%, as shown in the overall energy diagram in Figure S16. For PEG-based electrolytes, most of the internal resistance comes from interface resistance, with only a small fraction from bulk materials resistance. In the tunable TES device, a large amount of the PCM is needed to store thermal energy due in part to the high internal ohmic resistance, hence the low round-trip energy efficiency. The low round-trip energy efficiency is material specific. As in the PEDOT-CNT cathode system, the low round-trip energy efficiency comes from both higher internal ohmic resistance and low Coulombic efficiency of the DIB; the cell requires 0.9 J electrical energy to charge the device, but only ~0.2 J electrical energy can be recovered upon discharge with a round-trip electrical energy efficiency of only ~20%. Therefore, there is much room for improvement of the tunable TES device in enhancing the round-trip electrical energy efficiency. In addition, the self-discharge of a fully charged cell is 0.2 V over 12 h at 25°C and may be reduced further by eliminating side reactions present in the device. As Li-ion batteries demonstrate slow self-discharge, the preliminary finding suggests that a constant applied voltage to the tunable TES device may ultimately not be necessary to maintain target transition temperatures for PCM applications.

The ΔH of pure PEO is 137.1 J/g and the melting point is 27.6°C (Figure 2). The highest salt concentration 47%LiODFB is at the far end of the tunability, with ΔH of 88 J/g and a melting point of 15.5°C. At the 2 extremes between pure PEO and 47% LiODFB, the tunability is 12.1°C (Figure 2), achieved in the static experiment in which ΔH reduces by ~35%. In the dynamic experiment, a moderate concentration of 30% LiODFB (Figure 3D, cells a–d) is used, in which ΔH is 120 J/g (Figure 2A) (i.e., it decreases by only 12.5%). The salt does decrease the ΔH of the PCM, but it remains within a reasonable range. In a prototype device, there is no need for a separator, as the PCM itself can act as a physical barrier between the two electrodes. The addition of the salts and electrical energy storage electrodes added additional weight to the tunable PCM device; however, they also provided additional functions for reversible electrical energy storage.

The overall energy efficiency of electrochemically modulated TES also depends critically on the frequency of thermal cycling and electrochemical cycling (see Method details). For example, the overall energy efficiency ε for cell a in Figure 3D for diurnal modulation of T_m based on Equation 2 (Method details) is $\varepsilon \approx 50\%$, assuming a round-trip thermal storage efficiency of $\eta = 90\%$ and a thermal energy capacity of $E_t = 1.7$ J, whereas for the seasonal modulation of T_m, this increases to $\varepsilon = 89\%$. If the electrical energy can be recovered, then the overall energy efficiency for the diurnal case increases to ~72%.

Two directions for the future tunable TES device can be further envisioned based on the current DIB design. As in the case of batteries, enhancing Coulombic efficiency and reducing interface resistance of the tunable TES device could improve the electrical round-trip energy efficiency to ~80%. The thermal energy storage and electrical energy storage capacity are similar in the case of PANI-CB, and the tunable TES device can be used concurrently as both a tunable TES device and a rechargeable electrical energy storage battery. Another direction is to further reduce voltage of the device to reduce electrical energy consumption for the operation of the tunable TES device.

Here, we demonstrate a much-needed tunable melting point PCM device combining thermal storage with electrical energy storage function. A swing of 12.1°C and 6°C is demonstrated across static and dynamic cases, respectively, for the fractional transition temperature T_{10}. Flory-Huggins theory was applied to different salt-PEG systems to understand the trend in the transition temperatures with different cation and anion sizes. It was found that large asymmetries between the cation and anion radii yield larger interaction parameters and greater degrees of transition temperature depression. This suggests that salts with high solubilities in PEG, such as alkali salts used for battery chemistries, are optimal for dynamic tunability applications. Although this demonstrates dynamically tuning the transition temperature, there are still many research and development (R&D) challenges that, if answered, can improve the performance dramatically. Some of those are listed here for future research directions: the selection of cathode and anode within the stability range of the electrode can significantly prolong device lifetime; the use of low-cost and naturally abundant materials can ensure scalability; and replacing Li-ion with Na-ion could completely eliminate the resource-constrained Li element. More specifically, Figure 3D shows that in the dynamic experiments, the lowest salt concentration achieved in PEG was ~30 mol % (cell a), which means that all of the salt in the PEG was not able to be stored in the electrodes. This was primarily due to the inability of the electrodes to hold more charge. The salt concentration in PEG can be reduced further by fabricating thicker electrodes with higher active material loading to increase their charge capacity, or by designing electrodes that use higher-capacity materials.

Materials development of the electrolyte is another promising area of research. An electrolyte that undergoes a solid-solid phase transition obviates the need for a matrix to encapsulate the PCM in the liquid state. From a higher-level perspective, electrolytes with a wider electrochemical stability window increase the number of chemistries available for dynamic tunability. One promising chemistry due to economic considerations is a graphite-graphite dual-ion battery, but it would require an electrolyte with an electrochemical stability window from 0 to 5 V versus Li/Li^+. Crucial to understanding device operation is relating the composition of the PCM electrolyte to its transition temperature. This work has relied on FHT to understand the effect of salt concentration on the transition temperature in static samples. Developing a theoretical model incorporating electrochemical effects may be more fruitful in designing the dynamic systems for tunable TES materials and devices.

EXPERIMENTAL PROCEDURES

Resource availability

Lead contact

Further information and requests for resources and reagents should be directed to and will be fulfilled by the lead contact, Ravi Prasher (rsprasher@lbl.gov).

Materials availability

PCMs and devices generated in this study will be made available on request, but we may require a payment and/or a completed materials transfer agreement if there is potential for commercial application.

Data and code availability

All data reported in this article will be shared by the lead contact upon request.

Polymer electrolyte synthesis

LiODFB (Sigma-Aldrich), LiTFSI (Sigma-Aldrich), LiI (Sigma-Aldrich), CsTFSI (Solvionic), and Pyr_{14}TFSI (Sigma-Aldrich) were purchased and dried under vacuum at

120°C for at least 12 h before storage in an Ar-filled glovebox (<1 ppm O_2/H_2O). PEG (M_n ~1,000; Sigma-Aldrich) was purchased and dried under vacuum at 60°C for at least 12 h before glovebox storage.

LiODFB-, LiTFSI-, LiI-, CsTFSI-, and Pyr_{14}TFSI-PEG samples were prepared in an Ar glovebox to minimize moisture contamination of the hygroscopic salts and polymer. The respective salts were mixed with melted PEG at 60°C in 15.5, 27.9, 38.1, and 46.5 mol% concentrations (equivalent to LiTFSI-PEG standards of 5, 10, 15, and 20 wt%, respectively) until a homogeneous solution was obtained. These salt-polymer concentrations are hereafter referred to using the mole percent as 16, 28, 38, and 47*X*-PEG, where *X* refers to the salt (e.g., 47LiODFB-PEG).

Electrodes and cell fabrication and electrochemical characterization

LTO electrodes were prepared using a doctor blade to cast a slurry of LTO (MTI Corporation), carbon black (Super C45, MTI Corporation), and PVDF (KF 9300, Kureha) in *n*-methyl pyrrolidone (NMP, Sigma-Aldrich) with a weight ratio of 80:10:10 on carbon-coated aluminum foil (MTI Corporation). Polyaniline (emeraldine base, M_n 50,000; Sigma-Aldrich), and carbon black (Denka) were thoroughly mixed before PANI-CB electrode fabrication. In a typical mixing, 100 mg polyaniline and 43 mg carbon black were added to a 200-mL ethanol solution. The materials were then sonicated until a homogeneous suspension was obtained (~1 h). The suspension was then centrifuged, and the product was dried in a vacuum oven at 70°C for 12 h. PANI-CB electrodes for initial materials characterization and validation were prepared using a slurry of PANI-CB and PVDF in NMP with a weight ratio of 70:30. Higher mass loading PANI-CB electrodes for the electrochemical device prototypes were cast into 304 stainless-steel 100 × 100 mesh. Electrodes were dried in air for 12 h before drying at 120°C under vacuum for at least 2 h. The areal mass loadings of LTO electrodes prepared using the doctor blade were 2–3 mg cm^{-2}, respectively. The areal mass loadings of the stainless-steel mesh PANI-CB electrodes were 7–10 mg cm^{-2}.

Electrochemical characterization was performed in 2032-coin cells using a Bio-Logic MPG-2 potentiostat. Half-cells were assembled in an Ar glovebox using Li-metal counter electrodes, 125-μm-thick PVDF separators (Durapore), and 47LiODFB-PEG. Before full-cell fabrication, LTO and PANI-CB electrodes were electrochemically cycled in half-cells to determine the operating voltage of the paired full cell. Full cells with PANI-CB were conditioned for 10 cycles before shown voltage curves. Unless otherwise noted, half-cells and full cells were cycled at 60°C to reduce the ionic resistance of the electrolyte and facilitate electrochemical cycling (the ionic conductivity of 47LiODFB-PEG is 6.4 × 10^{-7} and 3.3 × 10^{-4} S/cm at 25°C and 60°C, respectively).

Thermal characterization

DSC measurements were performed using a TA Discovery DSC 2500. Characterization of the salt-PEG samples was performed from −80°C to 60°C using a ramp rate of 10°C min^{-1}, with 10 min isothermal holds at the upper and lower vertex temperatures and repeated for multiple cycles to ensure reproducibility. To elucidate the contribution of kinetic limitations on the breadth of the peak in the DSC thermograms in the polymer electrolytes, step scans with 1°C increments with a ramp rate of 1°C min^{-1} and 30 min isothermal holds were performed through the phase transition region identified through initial characterization at 10°C min^{-1}. The average of the first five temperature intervals in the step scan measurements was

used to estimate the heat capacity of the samples for baseline subtraction. DSC sample preparation was carried out in a glovebox to avoid moisture contamination.

Ex situ characterization for dynamic experiments

They were performed on the PEG-infiltrated separator harvested from multiple full cells charged to different capacities. Full cells were cycled under galvanostatic conditions at currents corresponding to 20 mA/g unless otherwise noted, with a potentiostatic hold applied once the cell reached the upper voltage limit when mentioned (voltage hold cells). After cycling or a voltage hold, the cell was cooled to 0°C. This was done to lower the ionic conductivity of the polymer electrolyte and limit the self-discharge of the device. Cell disassembly and DSC sample preparation using the PVDF separators were carried out in a glovebox. Care was taken to remove excess LiODFB-PEG solidified on the separator and to harvest the PEG-infiltrated separator only where it was in direct contact with the electrodes.

Interaction parameter using FHT

Broadly speaking, the theory accounts for a change in the Gibbs free energy of the liquid phase of the polymer, ΔG, due to changes in the heat of mixing, ΔH_{mix}, and configurational entropy, ΔS_{config}. The enthalpy of mixing is characterized by the interaction parameter, χ, obtained by fitting the T_{50} curves using Equation 1[35]:

$$\frac{1}{T_m} - \frac{1}{T_m^0} = -\frac{R}{\Delta H_u}\frac{V_u}{V_1}\left(-\upsilon_1 + \chi\upsilon_1^2\right) \qquad \text{(Equation 1)}$$

where T^0_m and T_m are the melting temperature (taken here as T_{50}) of neat PEG and X-PEG, respectively; R is the gas constant; ΔH_u is the enthalpy of transformation of the polymer phase; V_u and V_1 are the molar volumes of neat PEG and the salt, respectively; and υ_1 is the volume fraction of the salt. Ideal molar volumes of the salts were calculated using the van der Waals radii of their respective cations and anions (Table S1). The ionic radius of $ODFB^-$ was not readily available, and the radius of bisoxalatoborate (BOB^-) was instead used as a rough approximation. Compared to using the physical molar volumes, the ideal molar volumes can help to account for differences in the atomic packing factors of the different salts.

The interaction parameter fits of the LiODFB-, LiTFSI-, CsTFSI-, and Pyr_{14}TFSI-PEG systems using the T_{50} temperatures of different static compositions are shown in Figure S2. The LiI-PEG system required a large positive χ to fit the increase in T_{50} at low concentrations and was omitted from further analysis. The negative values for LiODFB-, LiTFSI-, CsTFSI-, and Pyr_{14}TFSI-PEG systems indicate an exothermic heat of mixing of the salt and polymer.

Calculation of energy efficiency of the device

Figure S16 shows a schematic of energy flow in the device. T_m of the PCM is modulated electrochemically, and the electrical energy required for each modulation is E_e. Consider a process, which could occur over many months, during which T_m is modulated between a low and high value m number of times. If the electrical energy when the cell is discharged (higher salt concentration in PCM, lower T_m) is not harvested, then the total electrical energy input into the system is $m \times E_e$. During the same process, assume that the PCM is charged and discharged thermally n times and define the round-trip thermal efficiency as η. Then, the total useful thermal energy delivered from the PCM is $n \times \eta \times E_t$, where E_t is thermal energy required to thermally charge the PCM (for simplicity here, we assume that E_t is independent of T_m). Therefore, the overall energy efficiency (ε) of the system, defined as the useful thermal energy delivered as compared to the total energy input (thermal + electrical), is

$$\varepsilon = \frac{n\eta E_t}{nE_t + mE_e} = \frac{\eta}{1 + \frac{mE_e}{nE_t}}. \quad \text{(Equation 2)}$$

Equation 2 shows that the overall system energy efficiency depends fundamentally on two groupings: the ratio of thermal cycling and electrochemical cycling frequencies (m/n) and the ratio of electrical energy per T_m tuning cycle to thermal energy per PCM charge/discharge (E_e/E_t). The ratio m/n depends on the use condition and control strategy, while E_e/E_t depends on the device design and material properties. For example, if T_m is modulated diurnally and the PCM is thermally charging and discharging diurnally, then $m/n = 1$, whereas if T_m is modulated seasonally, then $m = 4$ (assuming 4 seasons) and n depends on how many times per day the PCM is thermally charging and discharging. Assuming that it charges and discharges thermally every day, then n = 365, so that now $m/n = 0.011$, which is 2 orders of magnitude improved compared to the case of diurnal m and n. This simple analysis shows that the requirements for E_e to be small compared to E_t are much stricter for diurnal modulation of T_m as compared to seasonal modulation; in fact, for seasonal modulation, even E_e as large as $\sim 10E_t$ may be perfectly acceptable. Note that to be conservative, Equation 2 has ignored the possibility of using the E_e when the cells are electrically discharged. More constructively, this device in principle can usefully store both electrical and thermal energy, and it would be possible to use the electrical energy when the cells are discharged, which will further increase the system energy efficiency. For this case, the energy efficiency is given by

$$\varepsilon = \frac{n\eta_t E_t + m\eta_e E_e}{nE_t + mE_e} \quad \text{(Equation 3)}$$

for diurnal case $\varepsilon = \frac{\eta_t E_t + \eta_e E_e}{E_t + E_e}$ and for seasonal case $\varepsilon = \frac{365\eta_t E_t + 4\eta_e E_e}{365E_t + 4E_e} \approx \eta_t$.

Calculating the LiODFB concentration in PEG in the dynamic cell from charge capacity measurement

The number of moles (x) of LiODFB in the electrodes for a given charge capacity is given by

$$x\ mol \left(\frac{6.022 \times 10^{23}\ ion}{mol}\right)\left(\frac{1.602 \times 10^{-19}\ C}{ion}\right)\left(\frac{\mu Ah}{0.0036\ C}\right) = y\ \mu Ah$$

The mole percent of LiODFB in the PEG is calculated for known x by

$$\frac{(12.4 - x)\ \mu mol\ LiODFB}{(12.4 - x)\mu mol\ LiODFB + 14.2\ \mu mol\ PEG} = mol\%\ LiODFB \text{ in PEG},$$

where 12.4 and 14.2 μmol LiODFB and PEG are the starting molar mounts of material in a separator fully saturated with 47 LiODFB-PEG.

SUPPLEMENTAL INFORMATION

Supplemental information can be found online at https://doi.org/10.1016/j.xcrp.2021.100613.

ACKNOWLEDGMENTS

This work was supported by the Energy Efficiency and Renewable Energy, Building Technologies Program, of the US Department of Energy, under contract no. DE-AC02-05CH11231.

AUTHOR CONTRIBUTIONS

R.P. originally conceived the idea of dynamically tuning T_m. S.K., G.L., and R.P. further developed the idea of using ions to tune T_m. J.L. and J.K.P. fabricated the

cells and conducted the experiments. P.K., S.K., and D.L. helped with the experimental data analysis. D.L. developed the theoretical models. J.P. participated in the results analysis. C.D. participated in the overall research discussions and results analysis. G.L. and R.P. directed the project.

DECLARATION OF INTERESTS

The authors declare no competing interests.

INCLUSION AND DIVERSITY

While citing references scientifically relevant for this work, we also actively worked to promote gender balance in our reference list.

Received: July 15, 2021
Revised: September 1, 2021
Accepted: September 24, 2021
Published: October 20, 2021

REFERENCES

1. Albertus, P., Manser, J.S., and Litzelman, S. (2020). Long-Duration Electricity Storage Applications, Economics, and Technologies. Joule *4*, 21–32.
2. Koohi-Fayegh, S., and Rosen, M.A. (2020). A review of energy storage types, applications and recent developments. J. Energy Storage *27*, 101047.
3. Song, M., Niu, F., Mao, N., Hu, Y., and Deng, S. (2018). Review on building energy performance improvement using phase change materials. Energy Build. *158*, 776–793.
4. Peng, Y., and Cui, Y. (2020). Advanced textiles for personal thermal management and energy. Joule *4*, 724–742.
5. Stark, A.K., and Klausner, J.F. (2017). An R&D strategy to decouple energy from water. Joule *1*, 416–420.
6. Ling, Z., Zhang, Z., Shi, G., Fang, X., Wang, L., Gao, X., Fang, Y., Xu, T., Wang, S., and Liu, X. (2014). Review on thermal management systems using phase change materials for electronic components, Li-ion batteries and photovoltaic modules. Renew. Sustain. Energy Rev. *31*, 427–438.
7. Singh, S., Gaikwad, K.K., and Lee, Y.S. (2018). Phase change materials for advanced cooling packaging. Environ. Chem. Lett. *16*, 845–859.
8. Tas, C.E., and Unal, H. (2021). Thermally buffering polyethylene/halloysite/phase change material nanocomposite packaging films for cold storage of foods. J. Food Eng. *292*, 110351.
9. Agrawal, N., Agarwal, V., Joshi, G., and Mangal, U. (2019). Role of phase change materials for safe transportation of pharmaceutical goods. https://www.ipimediaworld.com/role-of-phase-change-materials-for-safe-transportation-of-pharmaceutical-goods/.
10. Miller, W., Shrestha, S., Childs, K., and Stannard, E. (2012). Field study and energy-plus benchmarks for energy saver homes having different envelope designs. https://www.aceee.org/files/proceedings/2012/data/papers/0193-000017.pdf.
11. Fang, M., and Chen, G.M. (2007). Effects of different multiple PCMs on the performance of a latent thermal energy storage system. Appl. Therm. Eng. *27*, 994–1000.
12. Lu, Q., Huberman, S., Zhang, H., Song, Q., Wang, J., Vardar, G., Hunt, A., Waluyo, I., Chen, G., and Yildiz, B. (2020). Bi-directional tuning of thermal transport in $SrCoO_x$ with electrochemically induced phase transitions. Nat. Mater. *19*, 655–662.
13. Wehmeyer, G., Yabuki, T., Monachon, C., Wu, J.Q., and Dames, C. (2017). Thermal diodes, regulators, and switches: physical mechanisms and potential applications. Appl. Phys. Rev. *4*, 041304.
14. Li, B., Kawakita, Y., Ohira-Kawamura, S., Sugahara, T., Wang, H., Wang, J., Chen, Y., Kawaguchi, S.I., Kawaguchi, S., Ohara, K., et al. (2019). Colossal barocaloric effects in plastic crystals. Nature *567*, 506–510.
15. Mischenko, A.S., Zhang, Q., Scott, J.F., Whatmore, R.W., and Mathur, N.D. (2006). Giant electrocaloric effect in thin-film PbZr(0.95)Ti(0.05)O3. Science *311*, 1270–1271.
16. Pecharsky, V.K., and Gschneidner, K.A.J. (1997). Giant agnetocaloric effect in Gd-5(Si2Ge2). Phys. Rev. Lett. *78*, 4494–4497.
17. Han, G.G.D., Deru, J.H., Cho, E.N., and Grossman, J.C. (2018). Optically-regulated thermal energy storage in diverse organic phase-change materials. Chem. Commun. (Camb.) *54*, 10722–10725.
18. Han, G.G.D., Li, H.S., and Grossman, J.C. (2017). Optically-controlled long-term storage and release of thermal energy in phase-change materials. Nat. Commun. *8*, 1446.
19. Henry, A., Prasher, R., and Majumdar, A. (2020). Five thermal energy grand challenges for decarbonization. Nat. Energy *5*, 635–637.
20. Liu, G., Reinhout, M., Mainguy, B., and Baker, G.L. (2006). Synthesis, structure, and ionic conductivity of self-assembled amphiphilic poly(methacrylate) comb polymers. Macromolecules *39*, 4726–4734.
21. Liu, G., Reinhout, M.T., and Baker, G.L. (2004). Nanoscale lithium ion conducting polyethylene oxide with self-attached insulating layers. Solid State Ion. *175*, 721–724.
22. Wang, M., and Tang, Y. (2018). A review on the features and progress of dual-ion batteries. Adv. Energy Mater. *8*, 1703320.
23. Rothermel, S., Meister, P., Schmuelling, G., Fromm, O., Meyer, H.W., Nowak, S., Winter, M., and Placke, T. (2014). Dual-graphite cells based on the reversible intercalation of bis(trifluoromethanesulfonyl)imide anions from an ionic liquid electrolyte. Energy Environ. Sci. *7*, 3412–3423.
24. Pell, W.G., and Conway, B.E. (2004). Peculiarities and requirements of asymmetric capacitor devices based on combination of capacitor and battery-type electrodes. J. Power Sources *136*, 334–345.
25. Ike, I.S., Sigalas, I., and Iyuke, S. (2016). Understanding performance limitation and suppression of leakage current or self-discharge in electrochemical capacitors: a review. Phys. Chem. Chem. Phys. *18*, 661–680.
26. Dunn, B., Kamath, H., and Tarascon, J.-M. (2011). Electrical energy storage for the grid: a battery of choices. Science *334*, 928–935.
27. Xu, K. (2004). Nonaqueous liquid electrolytes for lithium-based rechargeable batteries. Chem. Rev. *104*, 4303–4417.
28. Kou, Y., Wang, S., Luo, J., Sun, K., Zhang, J., Tan, Z., and Shi, Q. (2019). Thermal analysis and heat capacity study of polyethylene glycol (PEG) phase change materials for thermal energy storage applications. J. Chem. Thermodyn. *128*, 259–274.
29. Karaman, S., Karaipekli, A., Sarı, A., and Biçer, A. (2011). Polyethylene glycol (PEG)/diatomite

composite as a novel form-stable phase change material for thermal energy storage. Sol. Energy Mater. Sol. Cells *95*, 1647–1653.

30. Blundell, D.J., Beckett, D.R., and Willcocks, P.H. (1981). Routine crystallinity measurements of polymers by d.s.c. Polymer (Guildf.) *22*, 704–707.

31. Schick, C. (2009). Differential scanning calorimetry (DSC) of semicrystalline polymers. Anal. Bioanal. Chem. *395*, 1589–1611.

32. Zhou, H., and Wilkes, G.L. (1997). Comparison of lamellar thickness and its distribution determined from d.s.c., SAXS, TEM and AFM for high-density polyethylene films having a stacked lamellar morphology. Polymer (Guildf.) *38*, 5735–5747.

33. Olmedo-Martínez, J.L., Meabe, L., Basterretxea, A., Mecerreyes, D., and Müller, A.J. (2019). Effect of chemical structure and salt concentration on the crystallization and ionic conductivity of aliphatic polyethers. Polymers (Basel) *11*, 452.

34. Zhang, S.S. (2019). Lithium oxalyldifluoroborate as a salt for the improved electrolytes of Li-ion batteries. ECS Trans. *3*, 59–68.

35. Colbow, K.M., Dahn, J.R., and Haering, R.R. (1989). Structure and Electrochemistry of The Spinel Oxides $LiTi_2O_4$ and $Li_{4/3}Ti_{5/3}O_5$. J. Power Sources *26*, 397–402.

36. MacGlashan, G.S., Andreev, Y.G., and Bruce, P.G. (1999). Structure of the polymer electrolyte poly(ethylene oxide)(6): LiAsF6. Nature *398*, 792–794.

37. Armand, M. (1990). Polymers with ionic-conductivity. Adv. Mater. *2*, 278–286.

38. Homann, G., Stolz, L., Nair, J., Laskovic, I.C., Winter, M., and Kasnatscheew, J. (2020). Poly(ethylene oxide)-based electrolyte for solid-state-lithium-batteries with high voltage positive electrodes: evaluating the role of electrolyte oxidation in rapid cell failure. Sci. Rep. *10*, 4390.

39. Scrosati, B., and Garche, J. (2010). Lithium batteries: status, prospects and future. J. Power Sources *195*, 2419–2430.

40. Xie, J., Liang, Z.J., and Lu, Y.C. (2020). Molecular crowding electrolytes for high-voltage aqueous batteries. Nat. Mater. *19*, 1006–1011.

41. Whittingham, M.S. (2004). Lithium batteries and cathode materials. Chem. Rev. *104*, 4271–4301.

42. Placke, T., Rothermel, S., Fromm, O., Meister, P., Lux, S.F., Huesker, J., Meyer, H.W., and Winter, M. (2013). Influence of graphite characteristics on the electrochemical intercalation of bis(trifluoromethanesulfonyl) imide anions into a graphite-based cathode. J. Electrochem. Soc. *160*, A1979–A1991.

43. Kim, J., Kim, J.H., and Ariga, K. (2017). Redox-active polymers for energy storage nanoarchitectonics. Joule *1*, 739–768.

44. Le, T.H., Kim, Y., and Yoon, H. (2017). Electrical and Electrochemical Properties of Conducting Polymers. Polymers *9*, 150.

45. Moni, P., Lau, J., Mohr, A.C., Lin, T.C., Tolbert, S.H., Dunn, B., and Gleason, K.K. (2018). Growth temperature and electrochemical performance in vapor-deposited poly(3,4-ethylenedioxythiophene) thin films for high-rate electrochemical energy storage. ACS Appl. Energy Mater. *1*, 7093–7105.

46. Harding, J.R., Amanchukwu, C.V., Hammond, P.T., and Shao-Horn, Y. (2015). Instability of poly(ethylene oxide) upon oxidation in lithium–air batteries. J. Phys. Chem. C *119*, 6947–6955.

47. Reddy, K.R., Jeong, H.M., Lee, Y., and Raghu, A.V. (2010). Synthesis of MWCNTs-core/thiophene polymer-sheath composite nanocables by a cationic surfactant-assisted chemical oxidative polymerization and their structural properties. J. Polym. Sci. A Polym. Chem. *48*, 1477–1484.

48. Qin, Q., and McKenna, G.B. (2006). Melting of solvents nanoconfined by polymers and networks. J. Polym. Sci. B Polym. Physiol. *44*, 3475–3486.

49. Han, C., He, Y.-B., Liu, M., Li, B., Yang, Q.-H., Wong, C.-P., and Kang, F. (2017). A review of gassing behavior in Li4Ti5O12-based lithium ion batteries. J. Mater. Chem. A Mater. Energy Sustain. *5*, 6368–6381.

50. Ding, Y., Guo, X.L., Ramirez-Meyers, K., Zhou, Y.G., Zhang, L.Y., Zhao, F., and Yu, G.H. (2019). Simultaneous energy harvesting and storage via solar-driven regenerative electrochemical cycles. Energy Environ. Sci. *12*, 3370–3379.

51. Maye, S., Girault, H.H., and Peljo, P. (2020). Thermally regenerative copper nanoslurry flow batteries for heat-to-power conversion with low-grade thermal energy. Energy Environ. Sci. *13*, 2191–2199.